Bandwidth and efficiency improvement in sequential load modulated balanced amplifiers

Mohammad Moussa, Ayssar Serhan, Pascal Reynier, Dominique Morche, Alexandre Giry

Bandwidth and Efficiency Improvement in Sequential Load Modulated Balanced Amplifiers

Mohammad Moussa, Ayssar Serhan, Pascal Reynier, Dominique Morche, Alexandre Giry

CEA-Leti, Univ. Grenoble Alpes, France

{mohammad.moussa, ayssar.serhan, pascal.reynier, dominique.morche,alexandre.giry}@cea.fr

***Abstract* — This papers proposes a novel design methodology to enhance bandwidth (BW) and efficiency in single-input Sequential Load Modulated Balanced Amplifier (S-LMBA). It investigates the impact of lossy off-state impedance of the auxiliary devices on efficiency degradation at back-off (BO) power and discusses the optimum choice of the auxiliary stage's output matching network to minimize this impact. Additionally, a practical approach to extract the optimum main-to-auxiliary phase shift profile that maximizes bandwidth and efficiency is proposed. The proposed methodology is experimentally validated through the design and measurement of a 43dBm S-LMBA prototype. Between 3-4.2 GHz, the measured prototype achieves 42.1-43.5 dBm of P_{sat}, a drain efficiency (DE) of 56.5%-66% and 45%-53% at peak and 9-dB BO, respectively.**

***Keywords* —Efficiency, LMBA, load modulation, wideband.**

I. Introduction

To improve spectral efficiency and data rate, 5G systems use complex modulated signals with high instantaneous bandwidth. These signals exhibit high peak-to-average power ratio and require high back-off from the saturated power to achieve the required system linearity, which degrades the average efficiency of conventional PAs. In addition, 5G transceivers must address a large number of frequency bands which accentuate the efficiency-bandwidth trade-off in 5G PAs.

The load modulated balanced amplifier (LMBA) emerged as a promising solution to simultaneously address the BO efficiency and bandwidth challenges [1][2]. More specifically, the sequential LMBA (S-LMBA) variant has been introduced to improve DE at deep BO power levels [3]. Moreover, the design space of S-LMBA was extended in [4] by considering the main-to-auxiliary phase shift at the combiner plane as a design parameter. Furthermore bandwidth extension techniques based on continuous Class-F−1/Class-J and 2nd harmonic manipulation are proposed in [5] and [6]. Finally, the impact of lossless off-state impedance on BW and efficiency degradation in dual-input topologies has been studied in [7].

This paper is structured as follow. Section II reviews the S-LMBA architecture operation and highlights the importance of main-to-auxiliary phase shift control to achieve wideband operation. Section III describes the design methodology focusing on the optimum choice of the auxiliary stage's output matching network that mitigates the impact of the lossy off-state impedance of the auxiliary devices. In addition, a practical approach to extract and implement the optimal main-to-auxiliary phase shift profile in single input configuration is presented. Finally, the experimental validation of the proposed methodology is presented in section IV.

II. Theoretical Background

The block diagram of the S-LMBA architecture is shown in Fig. 1(a). The main and auxiliary (Aux_1 and Aux_2) PAs are connected to the 3-dB quadrature coupler through the output matching networks $\mathrm{OMN_m}$ and $\mathrm{OMN_a}$, respectively. In the following, the subscripts m, $\mathrm{a_1}$, $\mathrm{a_2}$, refer to the main, $\mathrm{Aux_1}$and $\mathrm{Aux_2}$ devices, respectively. Subscripts B and P denote the BO and peak power levels, respectively. Moreover, the subscript c distinguishes the voltages, currents, and impedances at the coupler's input from those at the devices' drain plane.

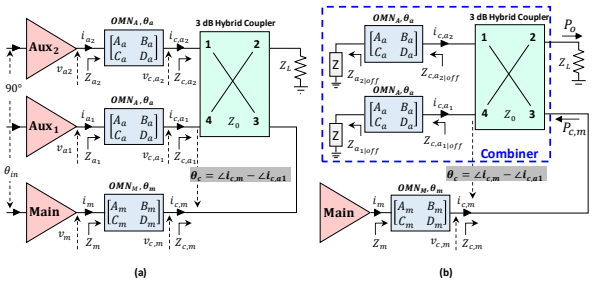

Fig. 1 (a) Block diagram of SLMBA, (b) Equivalent circuit of SLMBA at BO.

For a given target peak output power $P_{o|P}$ and peak to back-off power ratio ($\zeta = P_{o|P}/P_{o|B}$), the main PA delivers a constant output power (i.e. $P_{m|B} = P_{m|P} = P_{o|P}\,\zeta^{-1}$) across the BO region to the load Z_L. Note that the impedance seen at port-3 ($Z_{c,m}$) is constant and equal to the characteristic impedance of the coupler (Z_0) as long as $\mathrm{Aux_1}$ and $\mathrm{Aux_2}$ are driven in a balanced and quadrature manner and $Z_L = Z_0$. In the BO region, Aux1 and Aux2 are load modulated as follows:

$$Z_{c,a1} = Z_{c,a2} = Z_0\left(1 - j\sqrt{2}\left|\frac{i_{c,m}}{i_{c,a1}}\right| e^{j\theta_c}\right) \tag{1}$$

At $P_{o|P}$, $\mathrm{Aux_{1,2}}$ contribute equally to P_{out} and reach $P_{a1|P} = P_{a2|P} = 0.5(1-\zeta^{-1})P_{o|P}$. Moreover, the impedances seen by $\mathrm{Aux_{1,2}}$ at the combiner plane can be written as a function of Z_0, ζ and the phase shift θ_c ($\theta_c = \angle i_{c,m} - \angle i_{c,a1}$):

$$\mathrm{Z_{c,a1,2|P}}(\theta_c) = \frac{Z_0\left[\sin\theta_c + \sqrt{\zeta - \cos^2\theta_c} - j2\cos\theta_c\right]}{\sqrt{\zeta - \cos^2\theta_c} - \sin\theta_c} \tag{2}$$

It should be stressed that, for a given target back-off level ζ and a given choice of Z_0 there exists a continuum of $\mathrm{Z_{c,a1,2|P}}(\theta_c)$ values that satisfy the SLMBA requirement at $P_{o|P}$. This property is explored in the proposed methodology to achieve

wideband operation by assimilating the change of the operating frequency (f_0) to the change in θ_c. In fact, if $Z_{c,a1,2|P}$ evolution over frequency follows the trajectory of $Z_{c,a1,2|P}$ versus θ_c, the S-LMBA will maintain its optimum performance. However, the phase variation over frequency of the output and input matching networks, and the nominal value of θ_c and θ_a impacts the S-LMBA performance at peak and back-off and must be carefully considered, as will be discussed in the next paragraphs.

III. Design and Optimization Methodology

This section describes the design and optimization of a 3-4.2 GHz S-LMBA with a target $P_{o|P} = 20$ W and $\zeta = 8$ (9dB). Based on the power budget relations defined previously, $P_{m|P} = 2.5$ W and $P_{a1,2|P} = 8.75$ W are calculated. The CGH4006S transistor is chosen for the Main and Aux devices. For $P_{out} \leq P_{o|B}$, the auxiliary devices are represented by their off-state impedance at drain plane ($Z_{a_{1,2}|off}$), as shown in Fig. 1(b). The DE at BO can be written as $DE_{BO} = \eta_m \cdot \eta_{comb}$, where η_m is the DE of the main PA, and η_{comb} is the combiner efficiency defined as the ratio between P_{out} and $P_{c,m}$. Under balanced operation, i.e. $Z_{a_1|off} = Z_{a_2|off}$, $Z_{c,m}$ is always equal to Z_0. Thus, η_m is not affected by $Z_{a_{1,2}|off}$. Therefore, DE_{BO} is mainly affected by η_{comb} which is related to $Z_{a_{1,2}|off}$ by:

$$\eta_{comb} = \frac{P_{out}}{P_{c,m}} = \frac{\left|Z_{c,a_{1,2}|off}{}^2 - Z_0^2\right|^2}{\left|Z_{c,a_{1,2}|off} + Z_0\right|^4} \qquad (3)$$

where $Z_{c,a_{1,2}|off}$ can be written as

$$Z_{c,a_{1,2}|off} = \frac{B_a(\theta_a,\theta_c) + Z_{a_{1,2}|off}\, D_a(\theta_a,\theta_c)}{A_a(\theta_a,\theta_c) + Z_{a_{1,2}|off}\, C_a(\theta_a,\theta_c)} \qquad (4)$$

Equations (3) and (4) suggests the existence of an optimum θ_a and θ_c that maximizes η_{comb}, for a given $Z_{a_{1,2}|off}$. For illustration, η_{comb} is plotted at 3.0 GHz and 4.2 GHz while sweeping θ_a and θ_c, Fig. 2. Note that the optimum load impedance of $Aux_{1,2}$ at drain plane ($Z_{a1,2|P}$) is extracted from load pull simulations under class-C bias ($V_{g,a1,2} = -5.2$ V) with $V_{dd,a1,2} = 32$ V. In addition, $Z_{a_{1,2}|off}$ is extracted from small-signal S-parameters under the same conditions. Moreover, the phase-controlled matching network synthesis technique in [8] is used to extract the network parameters (A_a, B_a, C_a, D_a) that match $Z_{c,a1,2|P}(\theta_c)$ to $Z_{a1,2|P}$ while controlling θ_a.

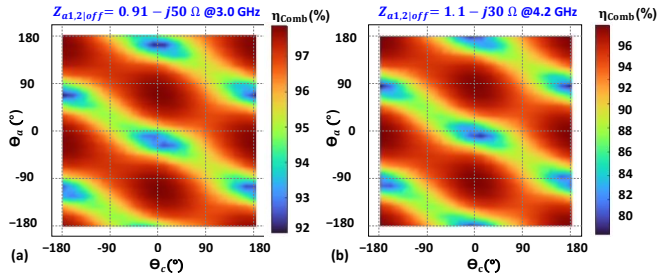

Fig. 2. η_{comb} versus $\theta_a \in [-180°, 180°]$ and $\theta_c \in [-180°, 180°]$ for $Z_0 = 50\ \Omega$, (a) at 3.0 GHz, (b) at 4.2 GHz.

Fig. 2 clearly shows the multiple optimum regions of θ_a and θ_c that maximize η_{comb}. Also, it shows that an arbitrary choice of θ_a and θ_c may reduce η_{comb} to 80%, thus degrading DE_{BO}. Note that in practice, θ_a and θ_c are frequency dependent and their variation over frequency cannot be easily formulated. In the following, a robust approach to select the nominal θ_a and θ_c values that maximize the SLMBA BW and DE under practical operating conditions is proposed.

First, a wideband main PA is designed. In practical scenario, the impedance $Z_{c,m}$ varies over frequency due to coupler phase and amplitude imbalances, especially when targeting wide frequency range. Therefore, the main PA is optimized to accommodate 1.6:1 VSWR load mismatch with respect to Z_0. The VSWR ratio is based on a pre-fabricated 3-dB coupler measurements data within the 3-4.2 GHz band. As shown in Fig. 3(a), when loaded with Z_0, the Main PA exhibits wideband performance with 34.5 dBm of P_{sat} with 71%-74.5% of corresponding peak DE in the targeted band. Moreover, Fig. 3(b) shows that the main PA maintains a DE>62% and P_{sat} >33.5 dBm when operating under 1.6:1 VSWR mismatch.

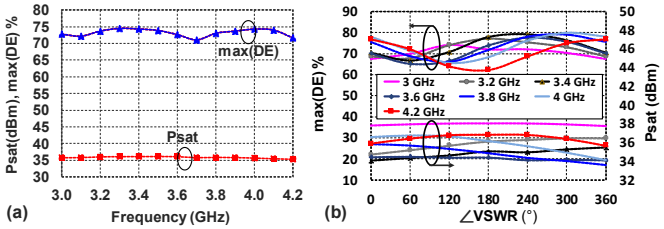

Fig. 3. Main PA peak DE and Psat: (a) under 50 Ω, (b) under a 1.6:1 VSWR.

Next, the auxiliary stage is designed. This step involves the optimal selection of OMN_a based on the choice of θ_a and θ_c. To better define this choice and consider the frequency response of the SLMBA, the equation based OMN_a (ABCD parameters) is transformed to a physical network as illustrated in Fig. 4. A series leg composed of a capacitor in series with a TL is used to compensate the imaginary part of $Z_{c,a1,2|P}$, resulting in a purely real impedance at plane A. Next, a series TL with a characteristic impedance equal to $\Re\{Z_{c,a1,2|P}\}$ is added to control the phase shift θ_a without affecting the impedance at plane B. Finally, the impedance at plane B is transformed to $Z_{a1,2|P}$ at the drain of the auxiliary device using an L-section.

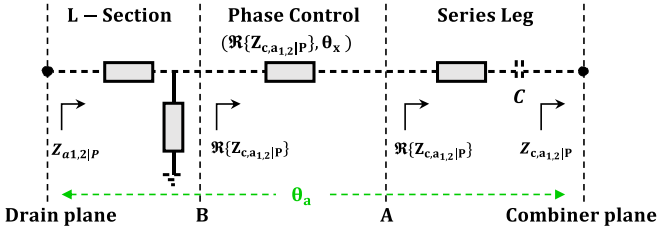

Fig. 4. A multi-section network approach to achieve a phase-controlled OMN_a.

For each combination of θ_a and θ_c where $\eta_{comb} > 90\%$, the dual-input configuration shown in Fig. 5(a) is used to extract the optimal phase shift $\theta_{in,opt}$ between the Main and Aux stage. This process involves sweeping the phase difference between the two inputs at each frequency within the targeted band.

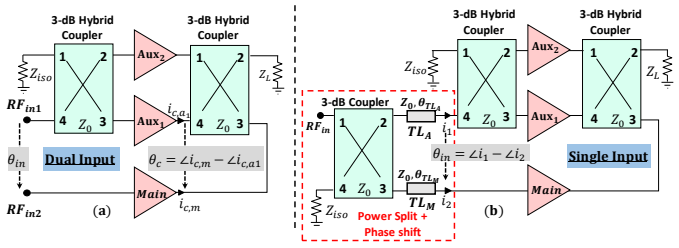

Fig. 5. Block diagram: (a) Dual input S-LMBA topology,(b) input power split associated with two TLs at the inputs of the main and Aux PAs .

The optimum combination of $\theta_{in,opt}$ profile, θ_a and θ_c is obtained using an iterative optimization process while setting the following goals at each frequency across 3-4.2 GHz: (1) achieving DE_{sat} >65%, (2) ensuring DE_{BO} >50%, (3) achieving P_{sat} =43±1dB, (4) maintaining DE>50% within the BO region. Note that the dual input extractions assume equal power split between the Main and Aux stages. Also, the input impedances of the main and auxiliary transistors are matched to $Z_0 = 50\Omega$. Fig. 6(a) - (b) and (e) show the DE, impedance trajectories, and the extracted $\theta_{in,opt}$ meeting the optimization goals with $\theta_a = 180°$ and $\theta_c = 60°$. The nonlinear evolution of the simulated θ_{in}, Fig. 6 (e), is caused by the impedance mismatch at the input of the auxiliary and main PAs. Moreover, Fig. 6 (b) shows that the simulated $Z_{c|a_{1,2}}$ (in red & pink) move towards the ideal $Z_{c,a1,2|P}$ trajectory predicted by (2) (in blue) at P_{sat} (i.e. $P_{o|P}$).

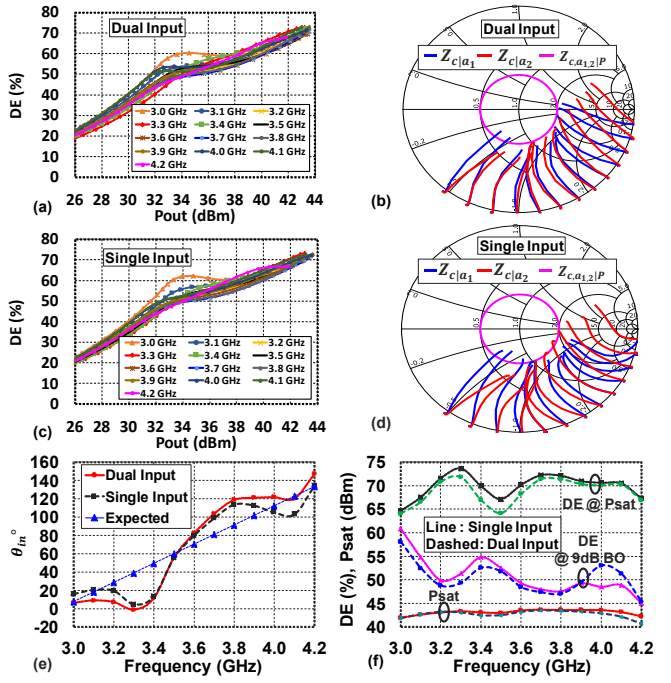

Fig. 6. Dual input SLMBA simulations: (a) DE%, (b) Impedances trajectories. Single input SLMBA simulations: (c) DE%, (d) Impedances trajectories. Dual versus single input SLMBA simulations: (e) θ_{in} (f) performance summary.

To achieve the desired $\theta_{in,opt}$ profile in single input configuration, the topology shown in Fig. 5(b) is considered. The input block, highlighted in red in Fig. 5(b), consists of a power splitter (3-dB hybrid coupler) and two TLs (TL_M and TL_A) serving as phase shifters. It can be shown that θ_{in} exhibits a linear evolution versus frequency as can be seen in (5):

$$\theta_{in}(f) = -90° - \frac{2\pi}{v_p}(l_M - l_A)\cdot f \tag{5}$$

where v_p denotes the phase velocity. In addition, l_M and l_A are the physical lengths of TL_M andTL_A, respectively. Equation (5) shows that the direction of θ_{in} evolution versus frequency is determined based on the sign of $(l_M - l_A)$. To achieve the increasing phase profile versus frequency extracted in dual input configuration, Fig. 6(e), l_M and l_A must satisfy the following condition:

$$l_A > l_M \Leftrightarrow \theta_{TL_A} > \theta_{TL_M} \tag{6}$$

First, the length of TL_M is fixed in light of layout floor planning considerations, resulting in θ_{TL_M}=200° at 3.6GHz. Next, the electrical length θ_{TL_A} is swept between $[\theta_{TL_M}, \theta_{TL_M} + 360°]$, to meet the previously defined goals while satisfying (6). An optimal length θ_{TL_A}=520° at 3.6 GHz is identified, resulting in a θ_{in} profile and DE performance closely resembling the optimum values as shown in Fig. 7(a) and (b), respectively.

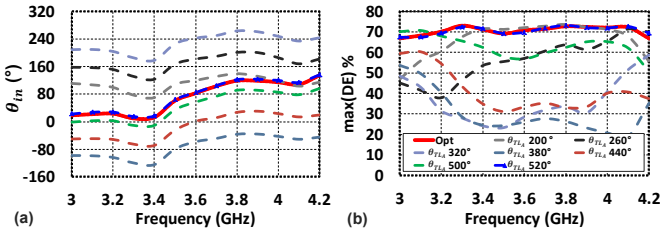

Fig. 7. Single input simulations: (a) θ_{in}, (b) maximum DE under θ_{TL_A} sweep for $\theta_{TL_M} = 200°$.

Fig. 6 (c)-(d) and (e) shows the DE versus P_{out} , the impedance trajectories, and the θ_{in} profile simulated in single input configuration. Moreover, the performance obtained in dual-input and single- input configuration at $P_{o|P}$ and $P_{o|B}$ are summarized in Fig. 6(f). These results validate the effectiveness of the proposed approach to achieve wideband operation in single-input configuration. The schematic of the optimized single input S-LMBA is shown in Fig. 8.

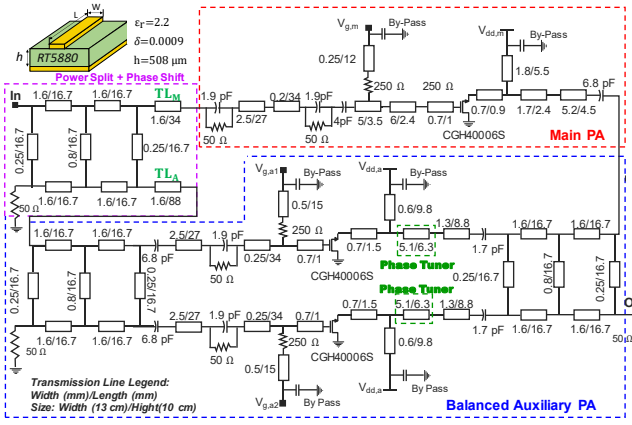

Fig. 8. Schematic of the proposed wideband single-input S-LMBA.

IV. Measurement Results

The proposed S-LMBA and the small-signal and large-signal measurements setup are shown on Fig. 9. The PA is implemented on a 20-mil Rogers Duroid-5880 PCB substrate ($\varepsilon_r = 2.2, \delta = 9e^{-4}$). The Main PA is biased in deep class-AB ($V_{g,m}$ =-2.8 V, I_{dc}=96 mA) with $V_{dd,m}$ =15 V, while the Aux stage is biased in class-C mode ($V_{g,a1}$ =-5.2 V, $V_{dd,a1}$ = 32V).

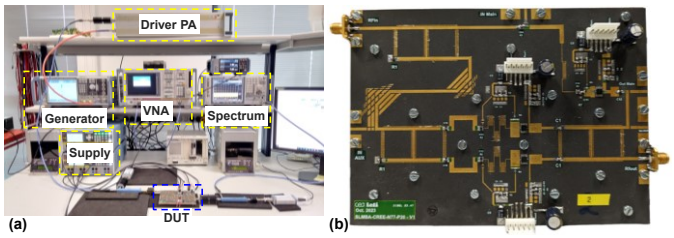

Fig. 9. (a) Photo of the measurement setup, (b) Photo of the fabricated S-LMBA (area=16.2x11.7 cm²).

Fig. 10 (a) shows good agreement between the measured and simulated S-parameters. As shown on Fig. 10 (b) and (c), from 3 to 4.2 GHz, the proposed PA delivers 42-43.5 dBm of P_{sat} with 56%-66% of corresponding DE and 45%-53% of DE at 9-dB BO. Moreover, Fig. 10 (d) shows that the PA can target different BO levels (8 to 12 dB) by adjusting $V_{dd,m}$ (12 to 20V) without compromising P_{sat} and DE at P_{sat} and BO powers.

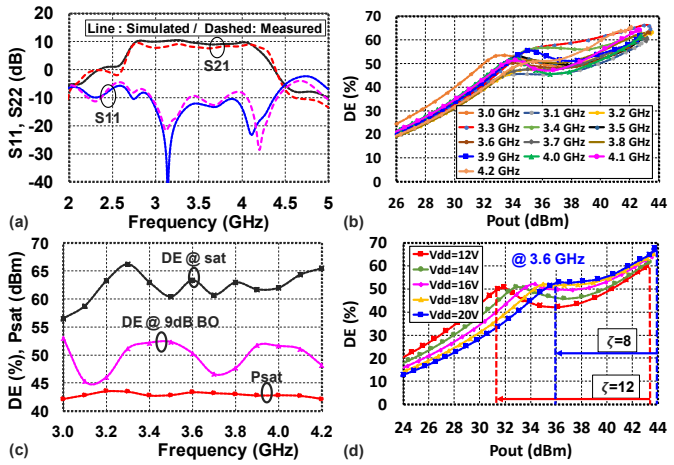

Fig. 10. Measurements under CW excitation: (a) S-parameters, (b) DE, (c) performance summary, (d) DE under $V_{dd,m}$ sweep at 3.6 GHz.

Table 1. Comparison with load modulated PAs

Ref.	Freq. (GHz)	FBW (%)	P_{Sat} (dBm)	DE_{sat} (%)	BO (dB)	DE_{BO} (%)	Architecture
[5]	3.05 3.55	15.2	42.3 43.7	60.8 74.8	9	50.9 64.9	S-LMBA
[9]	3.1 4.2	30.1	47.5 48.7	47 58	10	47 61	Assymetrical S-LMBA
[10]	3.45 3.75	8.3	41.8 43.5	46* 62*	8.5	33.3 54.1	Doherty
[11]	3.4 3.8	11.1	48* 48.5*	50* 60*	7.5	52.7 53.6	Doherty
T.W	3 4.2	33.3	42.11 43.5	56.5 66.2	9	45 53	S-LMBA

* Graphically extracted.

Table 1 presents a comparison summary of the measured results in this work with recent load modulated PAs operating in the same frequency band. Our work achieves the widest FBW when compared to load modulated PAs operating within the same band, as reported in [5],[10] and [11]. In comparison to [9], our work shows higher efficiency at saturation while achieving a slightly higher FBW.

V. Conclusion

A practical design and optimization methodology for wideband single-input S-LMBAs is proposed. The optimum choice of the auxiliary stage's output matching network that mitigates the impact of the lossy off-state impedance of the auxiliary devices is discussed. Furthermore, a rigorous approach to extract and implement the optimum main-to-auxiliary phase shift profile that maximizes bandwidth and efficiency is described. The fabricated S-LMBA achieves 42-43.5 dBm of P_{sat} with 56%-66% of corresponding DE and 45%-53% of DE at 9-dB BO over 33% of FBW around 3.6GHz, validating the effectiveness of the proposed approach.

Acknowledgment

This work was supported by the ANR under the France 2030 program, grant NF-PERSEUS: ANR-22-PEFT-0004.

References

[1] D. J. Shepphard, J. Powell, and S. C. Cripps, "An Efficient Broadband Reconfigurable Power Amplifier Using Active Load Modulation," in *IEEE Microwave and Wireless Components Letters*, vol. 26, no. 6, Jun. 2016, doi: 10.1109/LMWC.2016.2559503.

[2] R. Quaglia and S. Cripps, "A Load Modulated Balanced Amplifier for Telecom Applications," *IEEE TMTT*, vol. 66, no. 3, pp. 1328–1338, Mar. 2018, doi: 10.1109/TMTT.2017.2766066.

[3] J. Pang et al., "Analysis and Design of Highly Efficient Wideband RF-Input Sequential Load Modulated Balanced Power Amplifier," in *IEEE TMTT*, vol. 68, no. 5, pp. 1741–1753, May 2020, doi: 10.1109/TMTT.2019.2963868.

[4] Y. Cao and K. Chen, "Pseudo-Doherty Load-Modulated Balanced Amplifier With Wide Bandwidth and Extended Power Back-Off Range," *IEEE TMTT*, vol. 68, no. 7, Jul. 2020, doi: 10.1109/TMTT.2020.2983925.

[5] C. Chu et al., "Waveform Engineered Sequential Load Modulated Balanced Amplifier With Continuous Class-F−1 and Class-J Operation," in IEEE *TMTT*, vol. 70, Feb. 2022, doi: 10.1109/TMTT.2021.3123678.

[6] C. Chu, J. Pang, R. Darraji, S. K. Dhar, T. Sharma, and A. Zhu, "Broadband Sequential Load Modulated Balanced Amplifier With Extended Design Space Using Second Harmonic Manipulation," in IEEE *TMTT* , vol. 71, no. 5, May 2023, doi: 10.1109/TMTT.2022.3226440.

[7] C. Belchior, L. C. Nunes, P. M. Cabral, and J. C. Pedro, "Sequential LMBA Design Technique for Improved Bandwidth Considering the Balanced Amplifiers off-State Impedance," in IEEE *TMTT*, 2023, doi: 10.1109/TMTT.2023.3241690.

[8] R. Sinha and A. De, "Theory on Matching Network in Viewpoint of Transmission Phase Shift," in IEEE *TMTT*, vol. 64, no. 6, Jun. 2016, doi: 10.1109/TMTT.2016.2558645.

[9] P. Saad and R. Hou, "Symmetrical Load Modulated Balanced Power Amplifier With Asymmetrical Output Coupling for Load Modulation Continuum," in IEEE *TMTT*, vol. 70, no. 4, Apr. 2022.

[10] Y. C. Choi et al., "Doherty Power Amplifier with Extended High-Efficiency Range Based on the Utilization of Multiple Output Power Back-Off Parameters," in IEEE *TMTT*, vol. 70, no. 4, Apr. 2022, doi: 10.1109/TMTT.2022.3147843.

[11] X. A. Nghiem and J. Gajadharsing, "Continuous Quasi-Load Insensitive Class-E Mode for Wideband Doherty Power Amplifiers," in IEEE/MTT-S IMS, 2023, doi: 10.1109/IMS37964.2023.10188219.